

Filament Eruption in NOAA 11093 Leading to a Two-Ribbon M1 Class Flare and CME

Vema Reddy¹ · Ram Ajour Maurya² · Ashok Ambastha³

© Springer ●●●●

Abstract We present multi-wavelength analysis of a two ribbon M1.0 class flare that occurred in NOAA Active Region 11093 on August 7, 2010. This event was extensively observed by the recent space borne instruments on board SDO in several wavelengths. Additional observational data was obtained from STEREO, RHESSI and also the ground based NSO/GONG $H\alpha$ network telescope. From these observations, we inferred an upward rising motion of inverse S-shaped filament lying along the polarity inversion line (PIL) originating at the main sunspot. This motion appears to have triggered the filament eruption subsequent to the reconnection. As a result overlying field lines expanded, exploded as CME and material ejection was observed along the flux rope in STEREO/EUVI-A. The flare ribbons moved with significantly smaller separation velocity as compared to previous reports but not much difference was found in the calculated reconnection rates from the standard flare model. We suggest that observed flux emergence might have caused the flux rope to rise, resulting in the tethers to cut, and reconnection to take place; in agreement with the tether cutting model.

Keywords: Active Regions, Magnetic Fields; Corona, Active; Flares, Dynamics

1. Introduction

Solar eruptions are energetic events occurring due to the explosive release of magnetic energy. Understanding the driver and trigger mechanism of these solar eruptions is a challenging ongoing research problem in solar physics. These events manifest as prominence eruptions if seen at the limb, and filament eruptions if seen against the disk. They can be broadly divided into two classes - (i) ejective eruptions which give CMEs and long duration two-ribbon flares, and (ii) confined eruptions giving short duration flares. What defines the eruption to be ejective or confined remains an unanswered question. Reviews on theories of eruptions can be found in Lin, Soon, and Baliunas (2003), Priest and Forbes (2002).

¹Udaipur Solar Observatory (Physical Research Laboratory),
P.O. Box 198, Dewali, Badi Road, Udaipur 313 001, India.

¹ e-mail: vema@prl.res.in

² e-mail: ramajor@prl.res.in

² e-mail: ambastha@prl.res.in

Several ideas have been advanced for the eruption onset mechanism (Klimchuk, 2001; Forbes *et al.*, 2006; Moore and Sterling, 2006). In tether-cutting model proposed by Moore and Labonte (1980) and further elaborated by Moore *et al.* (2001), magnetic tension restraining the sheared core field of a bipolar magnetic arcade is released by internal reconnection above the polarity inversion line (PIL) of the arcade. Evidence for the tether-cutting model can be found in recent observational studies (Liu *et al.*, 2007; Wang, 2006; Yurchyshyn *et al.*, 2006). External tether cutting or “breakout” reconnection is similar to tether cutting in that it is a tension release mechanism via reconnection. But here it occurs between the arcade envelope of the erupting field and an over-arching restraining, reversed field of quadrupolar magnetic configuration (Antiochos, 1998; Antiochos, DeVore, and Klimchuk, 1999). Flux Cancellation (Martin, Livi, and Wang, 1985; Martin, 1989), emergence of twisted flux ropes from below the surface (Leka *et al.*, 1996), and ideal MHD instability (Kliem and Török, 2006; Fan and Gibson, 2007) are some other mechanisms proposed to explain the eruption process. Although there exist several proposed mechanisms, it is difficult in practice to disentangle as to which particular mechanism is responsible for fast eruption.

In filament eruptions, one commonly observed feature is two bright flare ribbons in chromospheric $H\alpha$ images, separating away as the flare progresses. Reconnection of magnetic fields is believed to be the underlying mechanism for energy release as proposed and studied by Carmichael (1964), Sturrock (1966), Hirayama (1974), Kopp and Pneuman (1976). As a coronal magnetic flux rope loses equilibrium and travels upwards, an extreme reconnection current sheet (RCS) is formed underneath. The reconnection in this RCS releases most of the magnetic energy stored in the magnetic field configuration (Forbes and Priest, 1984; Lin and Forbes, 2000). Charged particles can be effectively accelerated by the electric field in the RCS (Martens and Young, 1990; Litvinenko and Somov, 1995). Some particles, energized during a solar flare, gyrate around the field lines and propagate toward the underlying foot points, precipitating at different layers of the solar atmosphere to produce the two ribbon flares. Separation of these chromospheric flare ribbons is believed to provide a signature of the reconnection process occurring high up in the corona. This is the picture of standard flare model. All eruption models lead to this standard model in the onset phase of eruption.

The filament eruption event reported in this paper occurred on 07 August 2010 and led to M1 class two-ribbon flare and a fast CME. Previous works (Liu *et al.*, 2007; Liu *et al.*, 2005; Wang and Sheeley, 1999) reveal the essence of high cadence and high resolution observations in multi wavelengths. Present work utilizes the opportunity of coordinated observations in multi wavelength channels in different atmospheric heights taken by Atmospheric Imaging Assembly (AIA) and Heliospheric Magnetic Imager (HMI) on board Solar Dynamic Observatory (SDO). We present a morphological study to find the triggering mechanism of the flare, and its energetics to quantify the flare characteristics. Possible conditions of eruption process due to flux emergence and cancellation is examined and the connection to flare and CME has been identified. The underlying conclusions are then compared with previous studies. The instrumental data and reduction techniques are presented in Section 2. Observations and

data analysis are described in Section 3 while Section 4 gives the summary and discussions.

2. INSTRUMENTAL DATA AND REDUCTION

The eruption event in NOAA solar active region 11093 ($N12^{\circ}E32^{\circ}$) occurred on 07 August 2010. It produced GOES class M1 flare starting at 17:55 UT and peaking at 18:25 UT. Observations of this event were covered by Atmospheric Imaging Assembly(AIA) and Helioseismic and Magnetic Imager (HMI) on board SDO as well as by the NSO/GONG $H\alpha$ network telescope at BBSO. The associated CME was detected by the COR1 coronagraph (Thompson *et al.*, 2003) on board both the Ahead and Behind satellites of the Solar TERrestrial RELations Observatory (STEREO) which were separated by about 150° . The flare associated with the CME was also detected by the Reuven Ramaty High-Energy Solar Spectroscopic Imager (RHESSI; Lin *et al.* (2002)).

AIA takes multi-wavelength images at $0''.6 \text{ pixel}^{-1}$ resolution and 12 s cadence. To study the flaring plasma, we focus on the images obtained by 94 Å (Fe XVIII; $\log T = 6.8$), 171 Å (Fe IX; $\log T = 5.8$) filters covering the upper transition region, and the 304 Å (He II; $\log T = 4.8$) filter covering the chromosphere and lower transition regions. To enhance the signal to noise ratio, images were added giving a cadence of 1 minute. We have used preprocessed images (level 1.0) provided after calibration involving bad pixel correction, aligning, and scaling.

HMI makes measurements of line-of-sight magnetic field of the full solar disk at 6173 Å with a resolution of $0''.6$ and 45 s cadence with a precision of 10G. We rotated images (level 1.0) for solar north pointing up, and scaling of data was done from header information. For increasing the signal to noise ratio, we added every four images to give a cadence of 3 min.

COR1 is an internally-occulted coronagraph of length $\sim 1.2\text{m}$ and is one of the STEREO SECCHI suite of remote sensing telescopes. It takes observations of CME from 1.3 to 4 solar radii in three different polarizing angles every five minutes. We have used *secchi_prep.pro* and *cor1_quickpol.pro* routines in STEREO software package to process the images and finally to get total polarization brightness images. For observing ejected material within $1.2 R_{\odot}$, we have also examined EUVI observations on board STEREO-A.

We obtained the $H\alpha$ 6563Å images of the AR from the NSO/GONG network telescope operating at BBSO that observes the Sun at a cadence of 1 min and $1'' \text{ pixel}^{-1}$ resolution.

All full disk images obtained from different instruments were aligned by differentially rotating to a reference image at 18:00 UT. The offset was corrected after remapping and by overlaying magnetic contours on images taken by different instrument. We have used standard SolarSoftWare(SSW) library routines for this study.

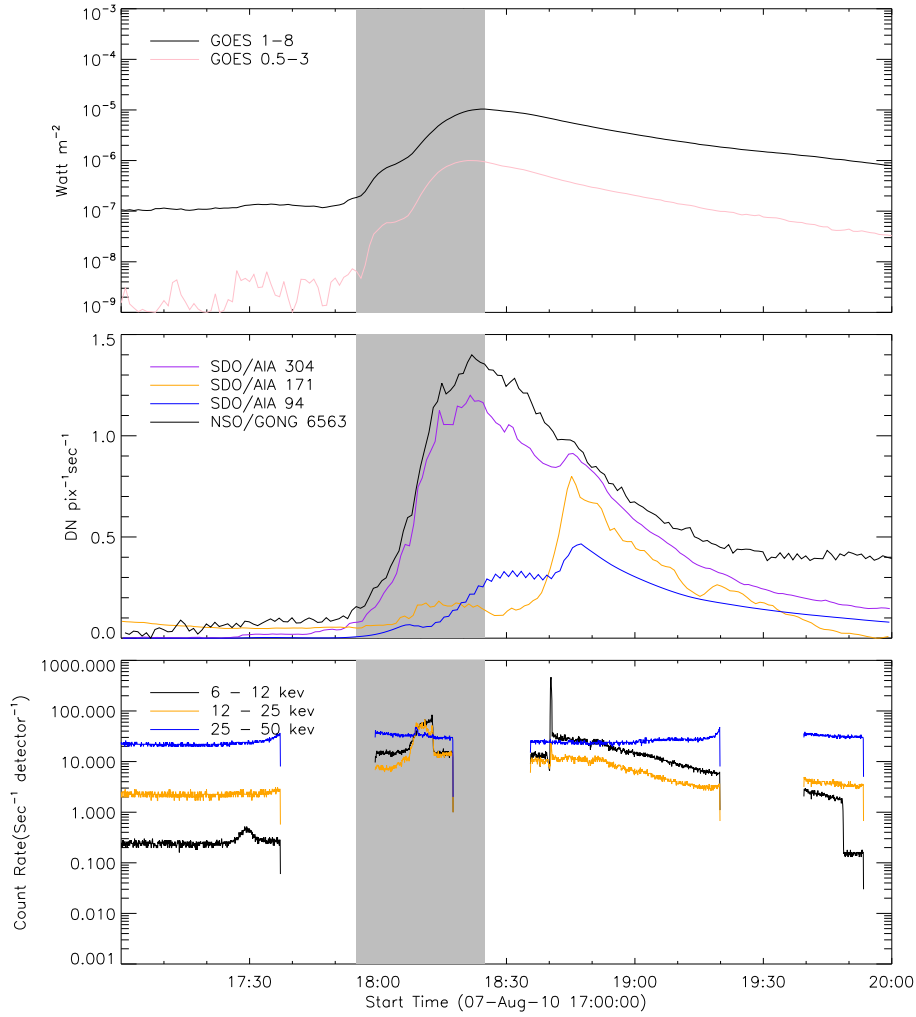


Figure 1. Light curves of the M1 class flare of August 7, 2010 in NOAA AR 11093: (top) GOES soft X-rays, (middle) AIA wavelengths and GONG $H\alpha$, and (bottom) RHESSI hard X-rays. Gray shaded region represents the impulsive phase of the flare as inferred from GOES soft X-rays. Gaps in RHESSI light curves are due to the spacecraft passage through night-times and the South Atlantic Anomaly.

3. OBSERVATIONS AND ANALYSIS

3.1. Filament Evolution Leading to the Two-Ribbon M1 Flare

3.1.1. Morphology

The active region NOAA 11093 consisted of an inverse S-shaped filament with one end connecting the sunspot observed in $H\alpha$ images many hours prior to

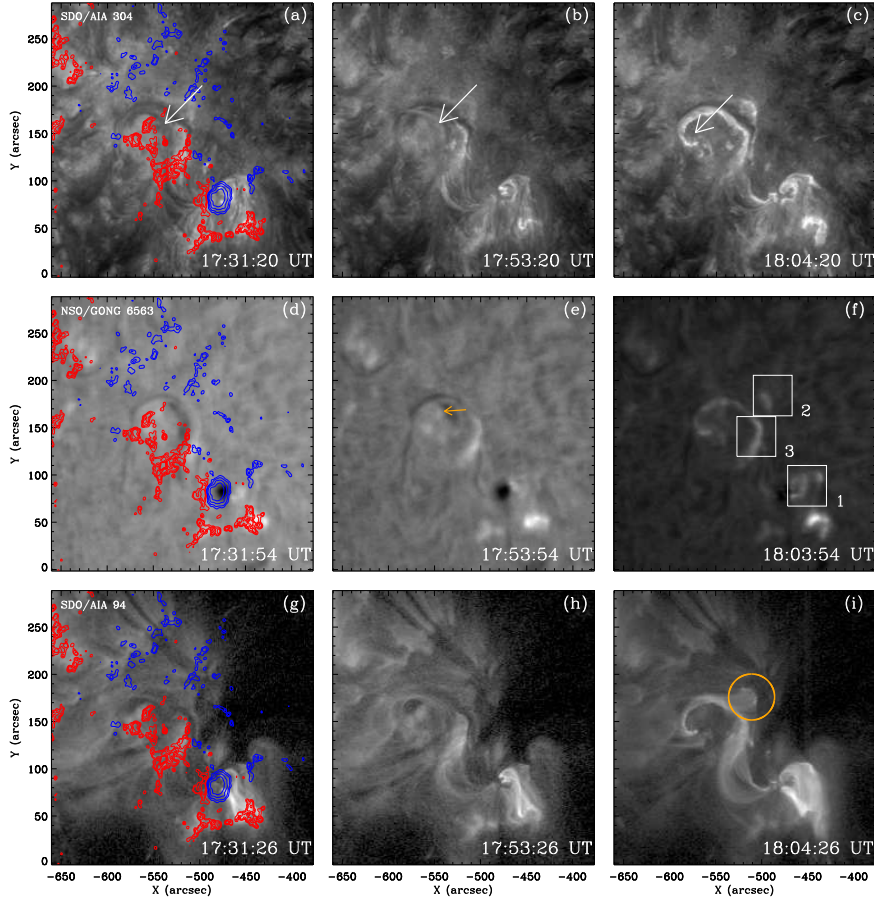


Figure 2. The images showing spatial and temporal evolution of the eruptive event. (Top row): AIA 304 Å images exhibit a rising motion of flux rope lying along PIL (marked by arrows). (Middle row) $H\alpha$ images show the corresponding chromospheric morphological changes. The boxes in frame ‘f’ mark the selected sites for intensity profile calculation. (Bottom row) AIA 94 Å images display the visible overlying field lines as the rope rises. In the left column, LOS magnetic field contours are overlaid with blue(red) colors marking the negative(positive) polarity fluxes.

start of the eruption. Light curves of the flare event in different wavelengths are plotted in Figure 1. The gray shaded region from the start to peak time of GOES flux represents the impulsive phase of the flare. From the peak time, the decay of GOES soft X-rays flux continued for over three hours which implies that it was a long duration event (LDE). The profiles in AIA 304 Å and $H\alpha$ followed the GOES X-rays. However, those in AIA 94 and 171 Å peaked with a significant delay of around 30 minutes. From the corresponding images, we found that these delayed peaks were related to the post-flare loops that appeared after the impulsive soft X-ray peak. There are gaps in RHESSI hard X-ray light curves due to the spacecraft passing through night-times and South Atlantic Anomaly.

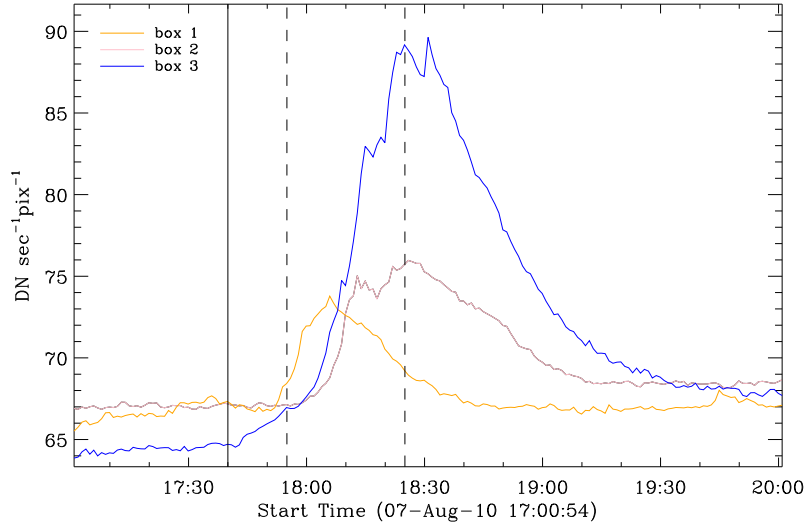


Figure 3. Temporal profiles of intensity obtained for the boxes marked in figure 2(f). There is a delay of 5-6 minutes in the start of brightening in boxes 2-3 lying on the flare ribbon as compared to the box 1 located near the sunspot. Solid vertical line marks the start time of rising flux rope and dashed vertical lines correspond to the start and peak times of the flare.

From movies made using the images in $H\alpha$ and AIA channels, we observed that a flux rope of an average diameter 6.89 Mm ($\sim 9''.5$) started to rise from the inner core of the filament at around 17:40 UT. Figure 2(a-c) shows, as pointed by arrows, the rise of flux rope connecting the sunspot and the other end of the filament elbow. The projection of this flux rope on the chromosphere is seen as dark shadow moving toward east and disappearing after 18:04 UT. At that time it had risen high, nearly vertical to the disk plane but was seen in EUVI images of STEREO-A as a limb ejected material. After 15 min from the start time of the rise, a brightening started to appear near the sunspot as flare ribbons; first the northern ribbon at the hump part and then the southern one. From the time of the rising GOES flux we infer that the flare phase began at 17:55 UT subsequent to the the rising motion of the filament. It is difficult at this point to suggest what actually triggered the rising motion of the flux rope. However, it is evident that this rising motion triggered the flare onset. We compare this to “tether cutting” model (Moore *et al.*, 2001). After the flux rope had risen to a certain height, the tethers in sheared core overlying along the filament were cut resulting in the reconnection of the inner magnetic field lines and initiation of the flare as evident from the increase of soft X-ray brightening.

From the line-of-sight magnetograms, we observed that the filament was oriented in a NE-SW direction along the polarity inversion line(PIL). Concerning the observed filament, the active region was quadrupolar with two main leading polarities located on either side of PIL, and two small following polarities of same sign. We have not considered the sunspot’s polarity for accounting the magnetic configuration of the region even though the filament rope was originating from it. We concentrate mainly on the time range 17:00–20:00 UT for studying the

changes occurring in morphological structure as well as field-line connectivity as the AR evolved with time.

We suggest that this motion is associated with the changes occurring near the sunspot which acted as a cause for triggering the subsequent process. To demonstrate this, we selected two small boxes of size $41'' \times 41''$ near the sunspot “1” and at the flare ribbon locations “2” and “3”. Temporal evolution of averaged intensity of these boxes is shown in figure 3. It is inferred that there is a significant delay between the peak brightening at the two sites. This remote brightening is due to reconnection of field lines from sunspots penumbra as evident from the EUV images. This is possible only when there is new flux emergence in the penumbra. Penumbral flux emergence was discovered first by (Zirin and Wang, 1993). This kind of new flux emergence can produce a so called magnetic channel, which is an elongated magnetic structure with alternating magnetic polarities and strong transverse magnetic fields along the channels. It should be noted that flux rope which is originating from the sunspot is also one of the magnetic channel.

Figure 4 is a mosaic of filament evolution, eruption and the flare in $H\alpha$ and the AIA channels in different wavelengths corresponding to different atmospheric layers (from left to right columns). The rows correspond to the time of start (top), impulsive (second and third), and decay (bottom) phases. The decay phase spanned over more than two hours. First column contains $H\alpha$ observations showing flare ribbons on the chromosphere. With time ribbons grew brighter and separated away up to peak time 18:25 UT and there after decayed. Images in the second column correspond to AIA 304 Å channel and show flare ribbons on the chromosphere as well as the overlying field lines filled with plasma at the temperature of $6 \times 10^4\text{K}$. Post-flare loops are clearly seen in the decay phase connecting the two ribbons. In third column, AIA 171 Å channel images show plasma loops more clearly as these are sensitive to $6 \times 10^5\text{K}$. Fourth column corresponds to AIA 94 Å channel images showing plasma loops in the coronal heights. From the movies constructed using these images, we observed twisted field lines in the inner core of filament at 18:06:02 UT turning to less twisted arcade loops in the decay phase at 19:06:26 UT.

From RHESSI light curves, it is evident that hard X-ray sources were produced during the flare. Unfortunately no data was available during 18:11-18:36 UT due to the spacecraft night-time and afterward too as attenuators were out of the field of view. The data was available only during 18:00-18:10 UT in the impulsive phase of the flare. We have constructed the images with “clean” algorithm from the modulated data and have looked for the sources of hard X-ray in the flaring region. In figure 5, we have plotted the contours of these reconstructed images in the energy bands of 3-6, 6-12 and 12-25 keV at 18:09 UT and overlaid on AIA 171 Å images. Integration time of the images was taken as 1 min, adequate to detect the changes. Due to the low count rates in this event, it was not possible to reconstruct images in higher energy bands. The contours were localized between the flare ribbon kernels suggesting that reconnection took place at these locations, where particles accelerated along the field lines toward foot points anchored on the photosphere. In 12-25 keV image, we observed a break in contours on ribbon hump part. This suggests that non-thermal hard

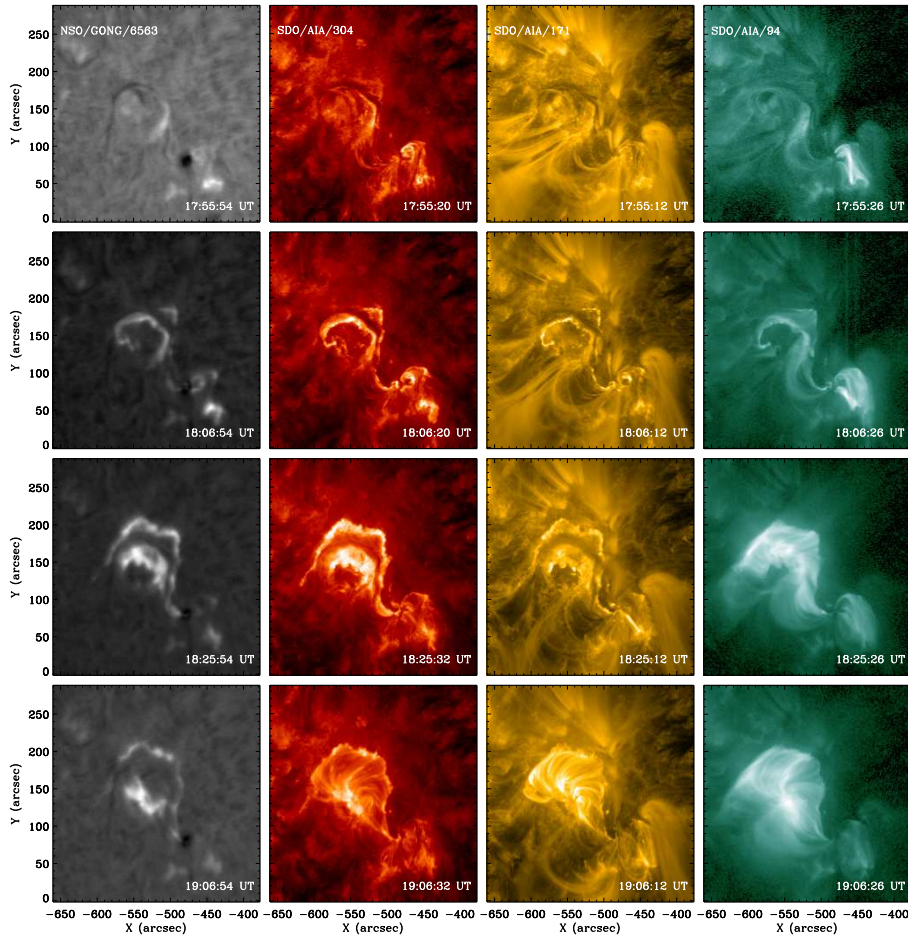


Figure 4. A mosaic of images showing the filament evolution during various phases of the flare – start (row 1), impulsive (rows 2 and 3), and decay (row 4) as observed in different wavelength channels corresponding to different atmospheric heights. (movie named “mosaic.mpeg” is available)

X-ray source were located at foot points on the flare ribbons. In the absence of additional HXR data, we are unable to follow up their evolution.

3.1.2. The Flare Energetics

We can study the flare energetics by two main physical parameters, viz., the rates of reconnection and energy release. Reconnection rate is the electric-field strength in RCS and is defined as the reconnected magnetic flux per unit time expressed as

$$\dot{\Phi} = B_c v_{in}. \quad (1)$$

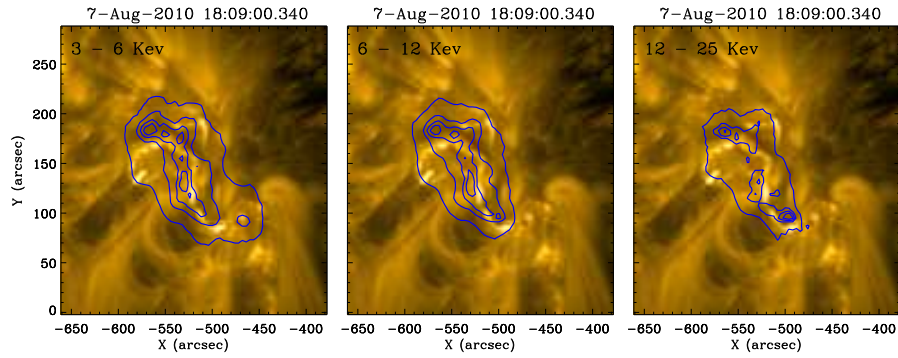


Figure 5. Contours of RHESSI hard X-rays overlaid on AIA 171 Å channel image at 18:09 UT in three energy bands: (left) 3-6 keV, (middle) 6-12 keV, and (right) 12-25 keV, reconstructed by clean algorithm with one minute integration time. Contour levels correspond to 50,70,80 and 90% of respective peak flux.

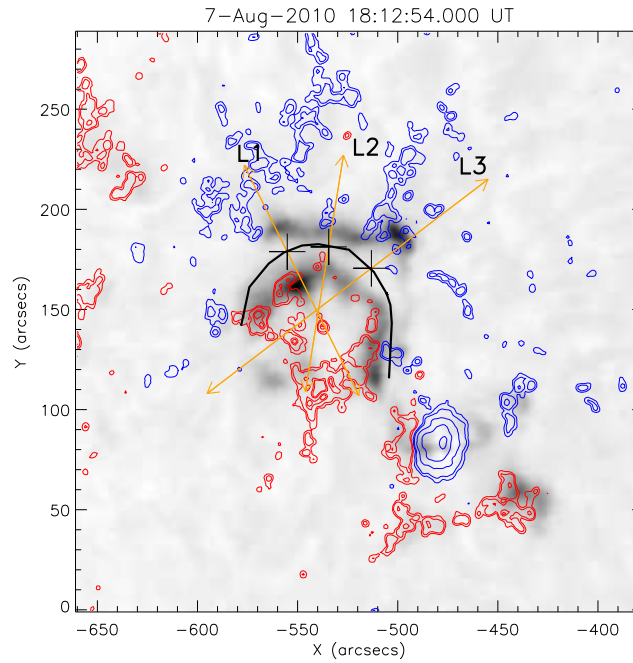


Figure 6. $H\alpha$ image of the flare (in negative) at 18:12:54 UT, overlaid with magnetic field contours. Solid black line is the simplified PIL. Arrowed lines L1, L2, and L3 drawn perpendicular to PIL at points marked by “+” follow the separation motion of the flare ribbons.

The magnetic energy release rate during a solar flare is the product of Poynting flux and the area of RCS that is generated during magnetic reconnection. On the basis of reconnection model, it has been shown by Isobe *et al.* (2002) that energy release rate can be written as,

$$\frac{dE}{dt} = SA_r f_r = \frac{1}{2\pi} B_c^2 v_{in} f_r, \quad (2)$$

where S is the Poynting flux into the reconnection region, B_c , v_{in} , A_r and f_r are coronal magnetic field strength, inflow velocity, area of the reconnection region, and the filling factor of reconnection inflow, respectively.

The inflow velocity can be determined from observations. Using the magnetic flux conservation theorem, one can write

$$B_c v_{in} = B_{\text{chro}} v_{\text{ribb}} = B_{\text{phot}} v_{\text{ribb}}, \quad (3)$$

where v_{rib} is the velocity of the $H\alpha$ ribbon separation, and B_{phot} , B_{chro} are the photospheric and chromospheric magnetic field strengths respectively.

Figure 6 depicts the scenario of flare ribbon separation motion along the lines L1, L2, and L3. We have measured distances from points shown by “+” on both sides of PIL shown in thick solid line, i.e toward the north and south directions. Separation velocities are then determined after fitting Boltzmann Sigmoids through the measured points. Using these, we further calculated the reconnection rates, and Poynting fluxes as plotted in Figure 7. For obtaining ribbons’ separation velocity, we followed the technique and assumptions presented in Maurya and Ambastha (2010) with $a = 0.2$ and $\epsilon = 0.4$. Reconnection rates were found to be in the range $0.1\text{--}0.3 \text{ kV m}^{-1}$ and Poynting fluxes in the range $0.008\text{--}3.8 \text{ G erg cm}^{-2} \text{ s}^{-1}$. Most profiles peaked within the time range of impulsive phase of the flare, but L3 south ribbon profile peaked out of this time since magnetic field dominated over the velocity. This flare lasted for about 3000 sec with current sheet spread over the area $\approx 10^{19} \text{ cm}^2$, with average energy release rate of $10^7 \text{ erg cm}^{-2} \text{ s}^{-1}$. Using these, we estimated the total energy released during this event at a modest value of 10^{29} ergs .

3.2. Changes in the Photospheric Magnetic field

Theoretical models suggest that evolution of magnetic fields at or below the photosphere, in the form of flux emergence and cancellation, could result in a loss of equilibrium of the magnetic structures (Martin, Livi, and Wang, 1985; Martin, 1989; Leka *et al.*, 1996). Changes in the photospheric longitudinal magnetic field around the time of eruption have been examined by many workers in the past (Martin, 1989; Wang and Sheeley, 1999; Mathew and Ambastha, 2000; Green *et al.*, 2003; Jiang, Shen, and Wang, 2007; Sterling, Harra, and Moore, 2007). Zhang, Zhang, and Zhang (2008) studied the relationship between flux emergence and CME initiation and inferred that 60% of CME source regions have magnetic flux increases and 40% have magnetic flux decreases. Here, we attempt to look for regions, if any, of flux emergence and cancellation in photospheric LOS magnetic field using the high resolution magnetograms from SDO/HMI.

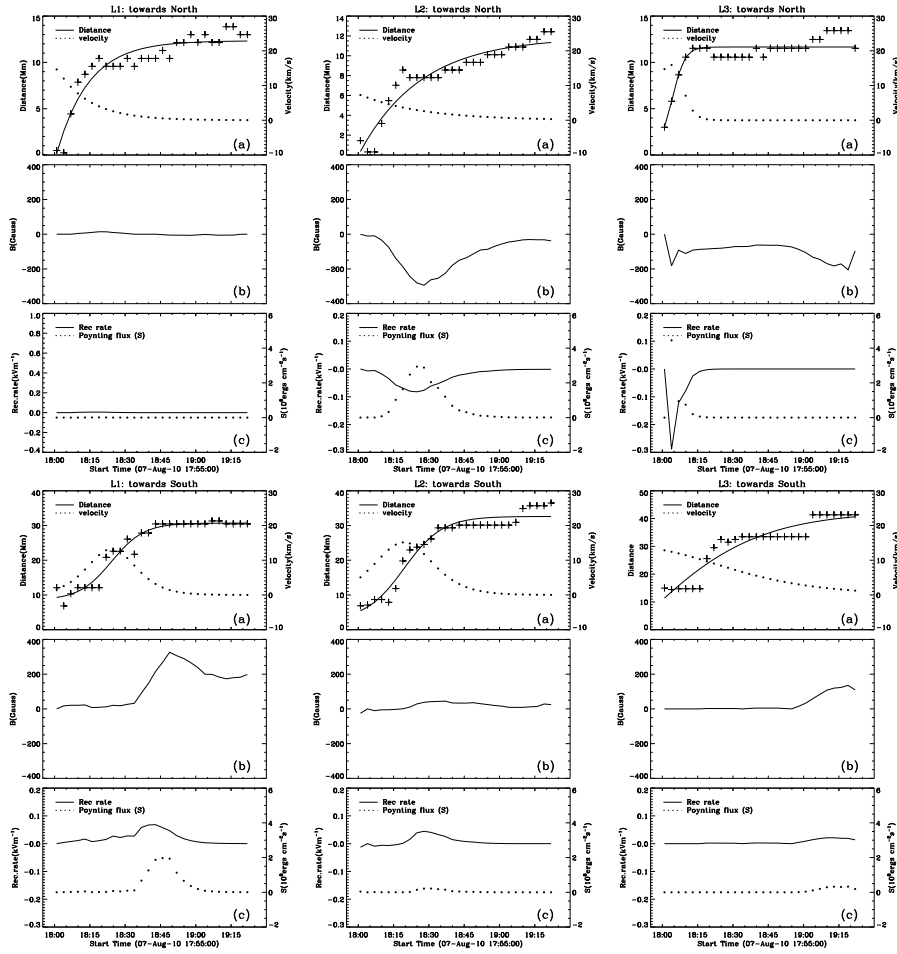


Figure 7. Various physical parameters calculated along the lines L1, L2 and L3 in the northern (top panel), and southern (bottom panel) directions. (a) “+” represents the measured distances of ribbons from PIL with time, and the solid lines through them represent Boltzmann sigmoid fits. The corresponding velocities are shown by dotted lines. (b) LOS magnetic field at the points of ribbon measurements, and (c) the reconnection rate (solid) and Poynting flux (dotted).

Registration of images was done by differentially rotating to a reference image at 18:00 UT. Effects of telescope jitter and other pointing errors were corrected by using a cross correlation method reducing the uncertainty within 1-2 arc sec. Every four images were added to yield 3min cadence. As the HMI precision is 10G, we have neglected magnetic fields below this value. From the movie made using the registered images, we detected three sites of flux emergence. In addition to these sites, we also selected sites where positive and negative polarities intruded into each other with a possibility of flux cancellation. A typical HMI magnetogram of NOAA11093 with the selected sites (boxes) and magnetic field contours is shown in figure 8 (left frame). Boxes 1 and 2 were selected to examine the changes due to the flux emergence in the sunspot penumbra as it evolved.

Boxes 3 and 4 were selected to examine flux cancellation by submergence or the opposite polarity fluxes intruding into each other. Boxes 5, 6 and 7 were sites of new flux emergence in the form of emerging bipoles, found by carefully observing the movie. Temporal evolution of total unsigned fluxes in these boxes is shown in Figure 8 (right frame) for about 4 hours covering the period before, during and after the flare/eruption. It is to note that sufficient care should be taken in selecting the box size: not too small or too big. A very small size box would not cover the area of interest adequately, and would give errors, while a too large area would dilute the magnitude of changes by averaging. Considering this, here we have chosen the boxes of size $30'' \times 30''$.

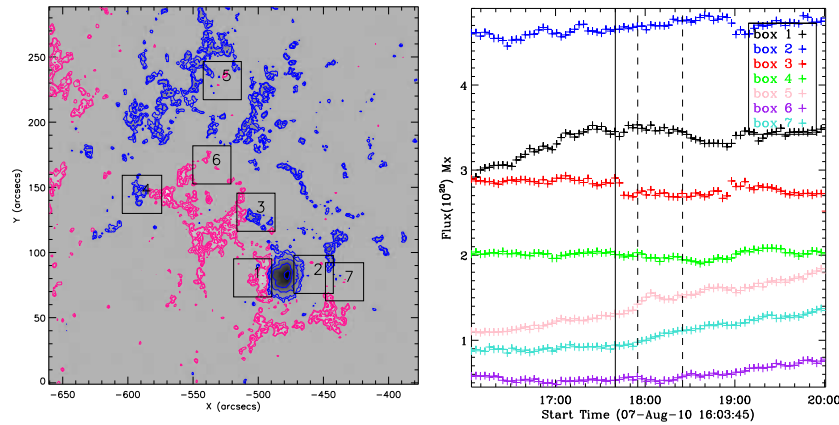


Figure 8. (Left) A LOS magnetogram of NOAA AR 11093 with contours of positive(negative) polarity in blue(red). Boxes mark the selected regions of interest for calculation of unsigned flux. (Right): Temporal profiles of unsigned flux in the regions of interest.

We interpret the observed flux profiles of each box and its contribution to the stability of magnetic system as follows: Boxes 1 and 2 are located around the leading sunspot. Box 1 covered the areas of opposite polarity fluxes and showed a rapid increase in total flux till the onset of the flare. It decreased afterwards in flare’s decay phase. Box 2, however, did not show significant changes. Boxes 3, 4, 5 and 6 are located at either side of the PIL from where field lines originated to tie the filament as ropes for a stable configuration. Changes, if any, in these boxes are important for stability of the filament. Boxes 3 and 4 were sites marked by intruding fluxes of opposite polarities. In box 3, there was an abrupt decrease of total flux by 0.2×10^{20} Mx at the time of flare onset as compared to that at the start of the rope rise. Flux in box 4, however, did not show appreciable changes. On the other hand, boxes 5, 6, and 7 exhibited increasing trend throughout with time, well beyond the event. Of these, box 6 was located underneath the flux rope. Thus, it is evident that there were several sites of flux emergence and cancellation in the filament and flaring regions that might have influenced the stability of the filament.

3.3. Filament Eruption and the CME

The rising flux rope started at 17:40 UT. It appeared as CME in the outer atmosphere (Figure 9). With its rise, we observed the surrounding overlying loops also rising as if they formed a balloon like cavity expanding temporally. In addition with this, EUV plasma ejection in the form of jet was observed as seen from STEREO A in 304 Å (Figure 9(c-f)). Because STEREO A and B were separated by 150°, and STEREO B was situated 71° west from Earth, AR 11093 was 36° west of STEREO B central meridian and 24° away from east limb of STEREO A. All these observational changes are well correlated in time with the flare phases. The jet like ejection of plasma came out from the reconnection region with ejection velocity proportional to the reconnection rate as its height increased. Eventually at about 18:20 UT, we observed it as CME event in the COR1 coronagraph.

Height-time analysis from triangulation method is a common practice in obtaining CME kinematics, such as, velocity, acceleration etc. We have constructed the observed distances of leading edge of the CME with time. In figure 9g, we have plotted distances from center of the Sun, in solar radii, with time. For reducing the errors of measurements, we have fitted the plot with a straight line. Slope of this line gives the velocity of CME as $574 \pm 23 \text{ km.s}^{-1}$. One should note that the measured distances were underestimates since the source region was not a limb event and the triangulation method does not take this departure into account. However, the velocity estimation is not affected by this difficulty.

4. SUMMARY AND DISCUSSION

In this study, we present a multi-instrument observation and analysis of NOAA 11093 in which an eruptive event occurred due to the reconnection of magnetic field leading to a fast CME and associated flare. Current models assume that the stored energy lies in a low lying magnetic flux system which is twisted or sheared. This system is the so-called core flux or flux rope. Such twisted systems in the form of inverse S or forward S shape, called sigmoids, are usually seen in association with eruptions. Canfield, Hudson, and McKenzie (1999) had studied the nature of activity with respect to morphology of eruptive or non-eruptive events with soft X-ray observations and inferred that sigmoids are more likely to erupt.

We attribute this eruption towards internal tether-cutting model even though the magnetic configuration is quadrupolar. Evidence for tether cutting reconnection in quadrupolar magnetic configuration was reported in Yurchyshyn *et al.* (2006). Rope started to rise around 17:40 UT from chromosphere and the brightening of ribbons, i.e., the onset of flare, started at 17:55 UT. By that time, the rope had already risen to the mid corona. In AIA 94 Å channels, we increasingly observed hot plasma filled, bright loops with time. These are possible only if the inner core field within filament structure overlying the PIL was to reconnect and released energy was to heat the plasma. As a result, reconnection site (loop top) arose, leading to the separation of ribbons. Thus we observed post-flare loops

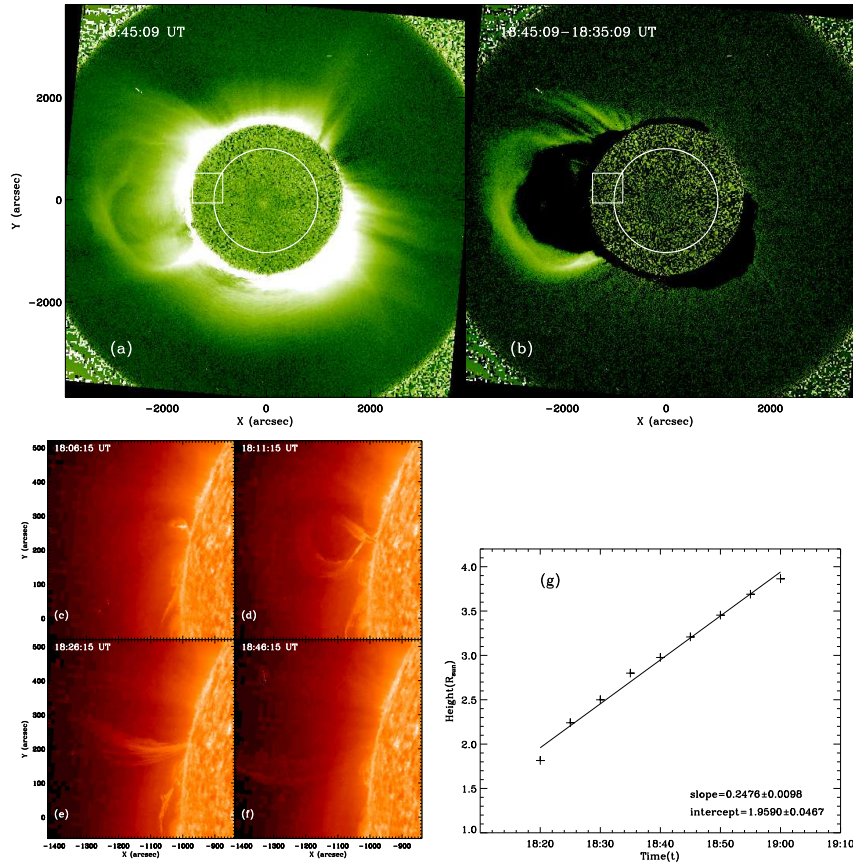


Figure 9. (a) The CME as observed by COR1 A at 18:45:09 UT. White circle represents the solar disk. (b) Difference image of the CME at 18:45:09 UT and 19:35:09 UT, (c)-(f): zoomed area of the box marked in ‘a’ showing the rising flux rope with time during the eruption observed by STEREO/EUVI-A in 304 \AA . (g) Fitted height-time plot of the CME within COR1 field of view.

connecting the flare ribbons 18:50 UT onwards in EUV wavelengths of 171 \AA , 304 \AA .

Further, the associated flare phases agreed well with standard flare model. The rising motion of rope had velocity of $8\text{-}9 \text{ km s}^{-1}$ and it took about 15 minutes to go into onset phase of flare/eruption. As a result overlying field lines expanded out and exploded as CME (figure 9a) with velocity $574 \pm 23 \text{ km s}^{-1}$ within the observed field of view. It appears unambiguously that material was supplied along the magnetic channel of this flux rope and it was ousted by ongoing reconnection into outer atmosphere (figure 9b). Flare ribbons were found to have maximum velocity in the range $12\text{-}16 \text{ km s}^{-1}$ and the reconnection rates in the range of $1\text{-}3 \text{ V cm}^{-1}$. These values are smaller as compared to the M3.9 flare event studied by Miklenic *et al.* (2007), who reported the values of $15\text{-}50 \text{ km s}^{-1}$ and $2.7\text{-}11.8 \text{ V cm}^{-1}$ for velocity and reconnection rates, respectively.

On the other hand, for a very short duration, impulsive C9.0 flare the same parameters are reported to have much larger values of 20-100 kms^{-1} and 90 $V\ cm^{-1}$ (Qiu *et al.*, 2002).

We now consider as to what triggered the eruption. Considering the flux emergence and cancellation as one of the prime causes, we examined the photospheric magnetic field changes occurring before, during and after the eruption. By a careful scrutiny of the high resolution HMI magnetogram movies, we found sites of flux emergence/cancellation around and across the PIL. The changes occurring in these sites are expected to have caused the loss of equilibrium of the magnetic structures and destabilized the flux rope. However, some instances of failed eruptions have been also reported even though there were flux emergence or cancellations. Another possibility is kinking of flux rope itself from the sunspot. A gradual increase in twist of the rope may eventually give rise to writhe causing the rope to rise (Kliem and Török, 2006), but from the available observations, it is difficult to comment on this possibility.

Acknowledgements The AIA(HMI) data used here are courtesy of SDO(NASA) and the AIA(HMI) consortium. We thank AIA team for making available processed data. This work utilizes data obtained by the Global Oscillation Network Group (GONG) Program, managed by the National Solar Observatory, which is operated by AURA, Inc., under a cooperative agreement with the National Science Foundation.

References

- Antiochos, S.K.: 1998, *Astrophys. J.* **502**, L181.
 Antiochos, S.K., DeVore, C.R., Klimchuk, J.A.: 1999, *Astrophys. J.* **510**, 485.
 Canfield, R.C., Hudson, H.S., McKenzie, D.E.: 1999, *Geophys. Res.* **26**, 627.
 Carmichael, H.: 1964, *NASA Special Publication* **50**, 451.
 Fan, Y., Gibson, S.E.: 2007, *Astrophys. J.* **668**, 1232.
 Forbes, T.G., Priest, E.R.: 1984, *Solar Phys.* **94**, 315.
 Forbes, T.G., et al.: 2006, *Space Sci. Rev.* **123**, 251.
 Green, L.M., Démoulin, P., Mandrini, C.H., Van Driel-Gesztelyi, L.: 2003, *Solar Phys.* **215**, 307.
 Hirayama, T.: 1974, *Solar Phys.* **34**, 323.
 Isebe, H., Yokoyama, T., Shimojo, M., Morimoto, T., Kozu, H., Eto, S., Narukage, N., Shibata, K.: 2002, *Astrophys. J.* **566**, 528.
 Jiang, Y., Shen, Y., Wang, J.: 2007, *Chinese J. Astron. Astrophys.* **7**, 129.
 Kliem, B., Török, T.: 2006, *Phys. Rev. Lett.* **96**(25), 255002.
 Klimchuk, J.A.: 2001, *Space Weather (Geophysical Monograph 125)*, ed. P. Song, H. Singer, G. Siscoe (Washington: Am. Geophys. Un.), 143 (2001) **125**, 143.
 Kopp, R.A., Pneuman, G.W.: 1976, *Solar Phys.* **50**, 85.
 Leka, K.D., Canfield, R.C., McClymont, A.N., van Driel-Gesztelyi, L.: 1996, *Astrophys. J.* **462**, 547.
 Lin, J., Forbes, T.G.: 2000, *J. Geophys. Res.* **105**, 2375.
 Lin, J., Soon, W., Baliunas, S.L.: 2003, *New Astron. Rev.* **47**, 53.
 Lin, R.P., et al.: 2002, *Solar Phys.* **210**, 3.
 Litvinenko, Y.E., Somov, B.V.: 1995, *Solar Phys.* **158**, 317.
 Liu, C., Lee, J., Yurchyshyn, V., Deng, N., Cho, K., Karlický, M., Wang, H.: 2007, *Astrophys. J.* **669**, 1372.
 Liu, Y., Su, J.T., Morimoto, T., Kurokawa, H., Shibata, K.: 2005, *Astrophys. J.* **628**, 1056.
 Martens, P.C.H., Young, A.: 1990, *Astrophys. J. Sup. Ser.* **73**, 333.
 Martin, S.F.: 1989, *Solar Phys.* **121**, 215.
 Martin, S.F., Livi, S.H.B., Wang, J.: 1985, *Australian J. Phys.* **38**, 929.
 Mathew, S.K., Ambastha, A.: 2000, *Solar Phys.* **197**, 75.
 Maurya, R.A., Ambastha, A.: 2010, *Solar Phys.* **262**, 337.

-
- Miklenic, C.H., Veronig, A.M., Vršnak, B., Hanslmeier, A.: 2007, *Astron. Astrophys.* **461**, 697.
- Moore, R.L., Labonte, B.J.: 1980, In: M. Dryer & E. Tandberg-Hanssen (ed.) *Solar and Interplanetary Dynamics, IAU Symposium* **91**, 207.
- Moore, R.L., Sterling, A.C.: 2006, *Washington DC American Geophysical Union Geophysical Monograph Series* **165**, 43.
- Moore, R.L., Sterling, A.C., Hudson, H.S., Lemen, J.R.: 2001, *Astrophys. J.* **552**, 833.
- Priest, E.R., Forbes, T.G.: 2002, *Astron. Astrophys. Rev.* **10**, 313.
- Qiu, J., Lee, J., Gary, D.E., Wang, H.: 2002, *Astrophys. J.* **565**, 1335.
- Sterling, A.C., Harra, L.K., Moore, R.L.: 2007, *Astrophys. J.* **669**, 1359.
- Sturrock, P.A.: 1966, *Nature* **211**, 695.
- Thompson, W.T., et al.: 2003, In: S. L. Keil & S. V. Avakyan (ed.) *Society of Photo-Optical Instrumentation Engineers (SPIE) Conference Series, SPIE Conference* **4853**, 1.
- Wang, H.: 2006, *Astrophys. J.* **649**, 490.
- Wang, Y., Sheeley, N.R. Jr.: 1999, *Astrophys. J.* **510**, L157.
- Yurchyshyn, V., Karlický, M., Hu, Q., Wang, H.: 2006, *Solar Phys.* **235**, 147.
- Zhang, Y., Zhang, M., Zhang, H.: 2008, *Solar Phys.* **250**, 75.
- Zirin, H., Wang, H.: 1993, *Nature* **363**, 426.